Contribution of axonal orientation to pathway-dependent modulation of excitatory transmission by direct current stimulation in isolated rat hippocampus

Anatoli Y. Kabakov, Paul A. Muller, Alvaro Pascual-Leone, Frances E. Jensen and Alexander Rotenberg

J Neurophysiol 107:1881-1889, 2012. First published 4 January 2012; doi:10.1152/jn.00715.2011

Journal of Neurophysiology publishes original articles on the function of the nervous system. It is published 12 times a year (monthly) by the American Physiological Society, 9650 Rockville Pike, Bethesda MD 20814-3991. ISSN: 0022-3077, ESSN: 1522-1598. Visit our website at http://www.the-aps.org/.

J Neurophysiol 107: 1881–1889, 2012.
First published January 4, 2012; doi:10.1152/jn.00715.2011.

Contribution of axonal orientation to pathway-dependent modulation of excitatory transmission by direct current stimulation in isolated rat hippocampus

Anatoli Y. Kabakov,[1] Paul A. Muller,[1] Alvaro Pascual-Leone,[2] Frances E. Jensen,[1] and Alexander Rotenberg[1,2]

[1]*Department of Neurology, Children's Hospital and* [2]*Berenson-Allen Center for Noninvasive Brain Stimulation, Beth Israel Deaconess Medical Center, Harvard Medical School, Boston, Massachusetts*

Submitted 1 August 2011; accepted in final form 3 January 2012

Kabakov AY, Muller PA, Pascual-Leone A, Jensen FE, Rotenberg A. Contribution of axonal orientation to pathway-dependent modulation of excitatory transmission by direct current stimulation in isolated rat hippocampus. *J Neurophysiol* 107: 1881–1889, 2012. First published January 4, 2012; doi:10.1152/jn.00715.2011.—Transcranial direct current stimulation (tDCS) is a method for modulating cortical excitability by weak constant electrical current that is applied through scalp electrodes. Although often described in terms of anodal or cathodal stimulation, depending on which scalp electrode pole is proximal to the cortical region of interest, it is the orientation of neuronal structures relative to the direct current (DC) vector that determines the effect of tDCS. To investigate the contribution of neural pathway orientation, we studied DCS-mediated neuromodulation in an in vitro rat hippocampal slice preparation. We examined the contribution of dendritic orientation to the direct current stimulation (DCS) neuromodulatory effect by recording field excitatory postsynaptic potentials (fEPSPs) in apical and basal dendrites of CA1 neurons within a constant DC field. In addition, we assessed the contribution of axonal orientation by recording CA1 and CA3 apical fEPSPs generated by stimulation of oppositely oriented Schaffer collateral and mossy fiber axons, respectively, during DCS. Finally, nonsynaptic excitatory signal propagation was measured along antidromically stimulated CA1 axons at different DCS amplitudes and polarity. We find that modulation of both the fEPSP and population spike depends on axonal orientation relative to the electric field vector. Axonal orientation determines whether the DC field is excitatory or inhibitory and dendritic orientation affects the magnitude, but not the overall direction, of the DC effect. These data suggest that tDCS may oppositely affect neurons in a stimulated cortical volume if these neurons are excited by oppositely orientated axons in a constant electrical field.

field excitatory postsynaptic potentials; paired-pulse facilitation; antidromic stimulation

TRANSCRANIAL DIRECT CURRENT stimulation (tDCS) is a well-tolerated technique for noninvasive neuromodulation supported by decades-old animal physiology data and recently applied in patients with a variety of neurologic disorders such as major depression, chronic pain, or epilepsy (Antal et al. 2011; Brunoni et al.; Dell'osso et al.; Kamida et al.; Lefaucheur et al. 2008; McFadden et al.; Nitsche et al. 2009; O'Connell et al.; Zaghi et al. 2009). During tDCS, cortical activity is modulated by prolonged (minutes) conductance of low-amplitude direct electrical current delivered through scalp electrodes. Applied to the mammalian cerebral cortex, cathodal tDCS induces an immediate and lasting (up to tens of minutes) decrease in excitability, whereas anodal tDCS increases excitability after a single session (Bindman et al. 1964; Nitsche and Paulus 2000). Yet, in contrast to other neurostimulation methods, tDCS amplitudes are insufficient to generate action potentials (APs) in the stimulated cortex (Purpura and McMurtry 1965), suggesting a mechanism of action more reliant on modulation of ongoing neuronal activity than induction of new neuronal activity (Cambiaghi et al. 2011; Fujiwara et al. 2011).

Cell membrane polarization in a static DC field is the most commonly cited neuromodulatory tDCS mechanism (Bikson et al. 2004). However, polarization of neuronal structures in a static electrical field will necessarily depend on the neuron's orientation relative to the extracellular electrical current vector (Bikson et al. 2004), and this is not uniform for all neurons in a stimulated brain volume. For example, two neurons may occupy the same stimulated region but may respond to the electrical field differently if the axon stimulating one is directed toward the cathode and the axon stimulating the other neuron is directed toward the anode.

To further elucidate the contribution of pathway orientation to tDCS-mediated neuromodulation, we reduced the tDCS technique to an in vitro hippocampal slice incubated in a constant DC electrical field (hereafter termed as "direct current stimulation," "DCS"). We tested an overall hypothesis that, in a constant electrical field, neuronal orientation will predict whether the applied external electrical current is inhibitory or excitatory. Specifically, we assessed how axonal or dendritic orientations contribute to the immediate DCS effect. We performed three main experiments. First, we tested the contribution of dendritic orientation to the DCS neuromodulatory effect by recording field excitatory postsynaptic potentials (fEPSPs) in a constant DC field but from oppositely oriented apical and basal dendrites in the CA1 hippocampal region. Next, we tested the contribution of axonal orientation by recording CA1 and CA3 apical fEPSPs generated by stimulation of oppositely oriented Schaffer collateral and mossy fiber axons, respectively, also in a constant DC field. Last, to further define the contribution of axonal orientation to the DCS effect, we studied nonsynaptic excitatory signal propagation along antidromically stimulated CA1 axons as we systematically varied the DC field polarity.

Address for reprint requests and other correspondence: A. Rotenberg, Dept. of Neurology, Children's Hospital Boston, 300 Longwood Ave., Boston, MA 02115 (e-mail: alexander.rotenberg@childrens.harvard.edu).

MATERIALS AND METHODS

Experimental animals. Litters of male P18–P24 Long-Evans hooded rats (10 pups/litter; Charles River Laboratories) were used to the study effects of DCS in isolated hippocampal slices. All animals were housed in a temperature-controlled animal care facility with a 12:12-h light-dark cycle. All procedures were performed in accordance with approval of CH Animal Care and Use Committee.

Hippocampal slice preparation. Hippocampal slices were prepared as described previously (Jensen et al. 1998; Sanchez et al. 2001). Briefly, rat pups were decapitated with all procedures in accordance with guidelines set by the institutional animal care and use committee. Brains were rapidly dissected from the skull and placed for sectioning in ice-cooled artificial cerebrospinal fluid (ACSF; in mM: 124 NaCl, 3.75 KCl, 1.25 KH_2PO_4, 2 $CaCl_2$, 2 $MgSO_4$, 26 $NaHCO_3$, and 10 D-glucose, pH 7.4, and bubbled with 95% O_2 and 5% CO_2 gas mixture). Coronal hippocampal slices (400 μm) were sectioned from the middle third of hippocampus with a manual tissue chopper (Stoelting, Wood Dale, IL) and transferred for 30 min to a chamber with oxygenated ACSF at 32°C and then to another slice chamber at room temperature for least for 1 h. Before recording, an individual slice was transferred to a flow-through interface chamber (BSC-HT; Harvard Apparatus, Holliston, MA) perfused with oxygenated (95% O_2-5% CO_2) ACSF at 40–50 ml/h and heated to 33.5°C (TC-344B; Warner Instruments, Hamden, CT). We deliberately used the interface chamber to have more accurate control of DC passing through the slice by minimizing DC electrical shunting via ACSF above the slice. In the interface chamber, the slice top protrudes from the ACSF surface and is exposed only to oxygenated water vapor. Electrophysiological recording started 1 h after slice transfer to the interface chamber.

DCS. DCS was applied via two silver-silver chloride electrodes with 1 mm diameter and 3 mm length (EP1; World Precision Instruments, Sarasota, FL) half-submerged in ACSF and connected to a constant-current stimulus isolator (A385RC; World Precision Instruments). The two DCS electrodes were positioned external to the hippocampal slice in one of two configurations such that the DC field would orient either orthogonal or parallel to the CA1 long axis (Fig. 1). To approximate in vivo tDCS terminology, we designated DCS as anodal or cathodal based on proximity of positive or negative DCS electrode, respectively, to the recording electrode. In this case, during cathodal DCS, the scalar product of the DC vector and the evoked AP propagation vector is positive, and during anodal stimulation the scalar product is negative.

Continuous monitoring of voltage at the site of the glass recording electrode revealed approximately linear dependence of the voltage on the DC amplitude. Maximal DCS amplitudes (−400 or +400 μA) corresponded to a slight increase in standard deviation of applied voltage up to 0.2 mV at −400 μA and up to 0.1 mV at +400 μA (Fig. 1, *A* and *B*) during 5 min of stimulation, but the voltage-current relationship overall remained linear within 10% when the voltage was measured by the recording glass electrode relative to a more remote DC electrode. The linear slope of the recording electrode voltage was 1.25 ± 0.09 mV/μA when two DC electrodes were positioned external to CA1 and CA3/dentate gyrus regions and 1.34 ± 0.03 mV/μA when the electrodes were positioned external to the CA2/CA3 and dentate gyrus region (Fig. 1). Given the 3-mm distance between the DC electrodes, the average electric field strength is ~40 V/m per 100 μA of DC, which is similar to the field strength in prior in vitro DCS publications (Bikson et al. 2004). We note that the highest anodal DCS (+400 μA), corresponding to the electric field strength of 160 V/m, often triggered spontaneous epileptiform activity, and therefore this condition was excluded from the experiments.

Because our experiment was aimed at investigating real-time DCS effects on excitatory transmission, we limited stimulation time to 5

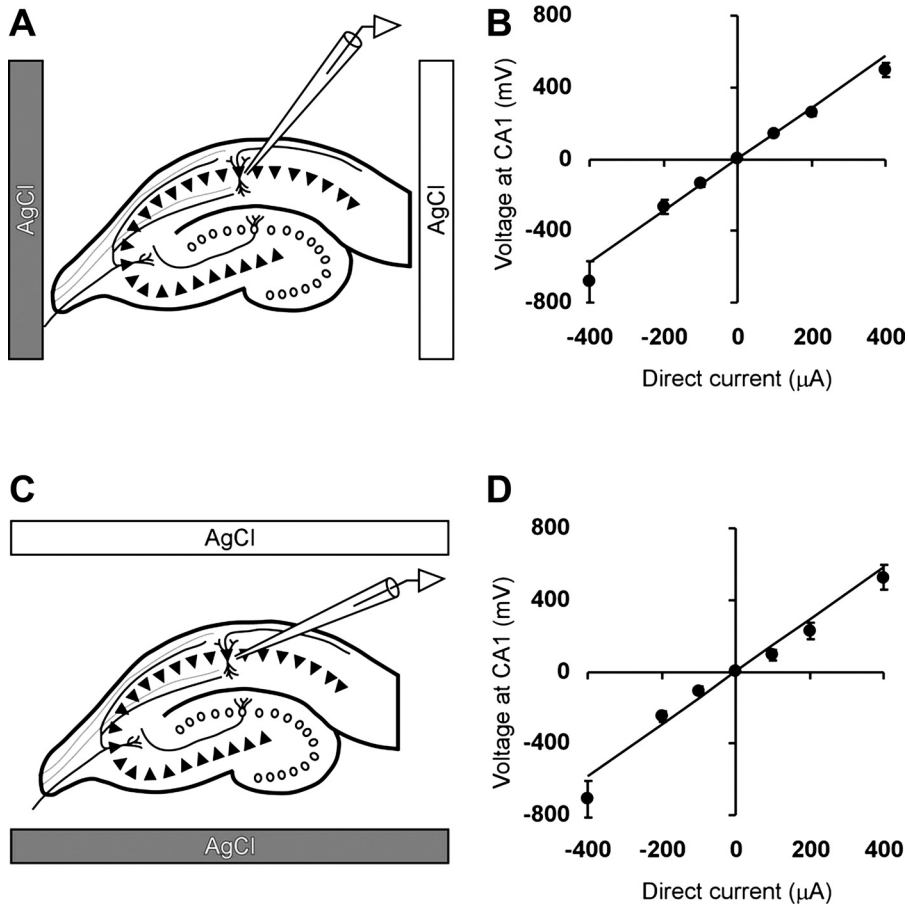

Fig. 1. Voltage inside CA1 layer nearly linearly depends on direct current (DC) amplitude. *A* and *C*: position of the recording electrode in CA1 region and positions of two DC silver-chloride (AgCl) electrodes in "horizontal" and "vertical" configurations, respectively. *B* and *D*: dependence of the voltage in CA1 region measured relative to the "gray" AgCl electrode as a function of the DC amplitude. Positive DC values correspond to positive potential of "white" DC electrode relative to gray DC electrode. Number of slices per condition is 6 or 7. Error bars correspond to SE.

min to avoid contributions of DCS to lasting changes in regional excitability. Also, to avoid the confounding contribution of abrupt changes in applied electrical current, data from the first three sampling stimuli were not included in the 5-min DCS block averages. Data from all active DCS blocks were compared with 15-stimuli (7-min) baseline recordings that were sufficient to provide stable baseline values for the responses during 5 min DCS as shown in Fig. 2.

Hippocampal slice electrophysiology. For recordings, we used glass (catalog no. 30–31-1; FHC, Bowdoinham, ME) microelectrodes filled with ACSF (1–2 MΩ), a model 1800 Microelectrode AC amplifier (A-M Systems, Carlsberg, WA), a data acquisition system (PCI bus; DataWave Technologies, Loveland, CO), DataWave SciWork software (DataWave Technologies), and an Axon Axopatch 200B amplifier, Digidata 1440A data acquisition system and pClamp 10 software (Molecular Devices, Sunnyvale, CA).

Axons were electrically stimulated through a platinum-iridium electrode (catalog no. CBBRC50; FHC, Chemnitz, Germany) placed in the regions of the Schaffer collaterals, stratum oriens afferent fibers, or mossy fibers, as detailed below. The amplitude of the 0.1-ms stimulus was always set to elicit 50% of the maximal response in the beginning of each experiment. The pulsatile test stimulus was applied every 30 s to evoke either a fEPSP or a population spike, depending on the experimental protocol. fEPSPs were recorded in CA1 stratum pyramidale, CA1 basal dendrite synapses, CA3 apical dendrite synapses, and the CA1 cell body layer as below. The effect of DCS on nonsynaptic excitatory transmission was determined with antidromic excitation of CA1 neurons by stimulation in the alveus while recoding population spikes in CA1 stratum pyramidale.

DCS modulation of paired-pulse facilitation (PPF) was measured by comparing the first and second fEPSPs in CA1 stratum pyramidale. Paired pulses were delivered with 50-ms interpulse intervals at 50% of the stimulus intensity that induced maximum response activity. The degree of facilitation was determined as the PPF ratio (second fEPSP/first fEPSP). Next, the PPF ratios during DCS were normalized to PPF ratios before DCS (PPF ratio at DCS/control PPF ratio).

Data analysis and statistics. All studied parameters (maximal fEPSP slope, PPF ratio, maximal population spike amplitude, and population spike peak latency) were normalized to respective baselines obtained before DCS. Per experimental condition, two means (the values obtained with DCS and the values obtained from the same slices with no DCS) were compared by two-tailed *t*-test. One-way ANOVA was used to test for the contribution of experimental condition (i.e., DCS intensity) to average peak fEPSP slope and population spike amplitude values. Differences with $P < 0.05$ were considered statistically significant. Experimental data in Figs. 1–8 and in the text are presented as means ± SE.

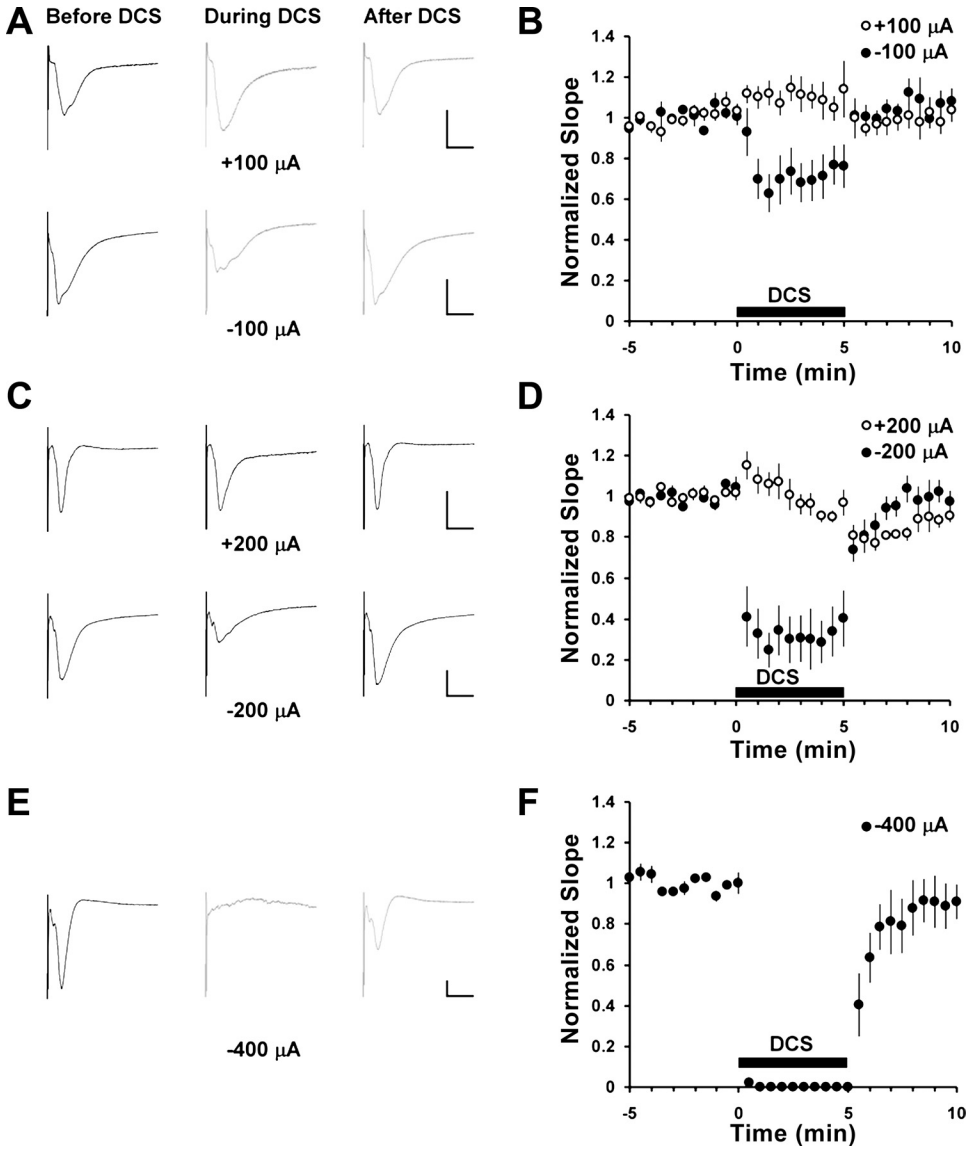

Fig. 2. Cathodal and not anodal direct current stimulation (DCS) significantly inhibits field excitatory postsynaptic potentials (fEPSPs) in the basal dendrites of CA1 neurons evoked by stimulation of association fibers in stratum oriens. *A*, *C*, and *E*: representative fEPSP recordings (averages of 7 consecutive traces) before (*left*), during (*middle*), and after (*right*) DCS at 100, 200, and 400 μA, respectively. DCS polarity was defined as the polarity of white DCS electrode relatively to gray electrode as shown in Fig. 1. The scaling bars correspond to 500 μV and 10 ms. *B*, *D*, and *F*: time courses of average values normalized to the baseline fEPSP slopes. DCS starts at *time 0* and ends after 5 min as shown by the filled bars. Open circles correspond to positive (anodal) DCS, and filled circles correspond to negative (cathodal) DCS. Numbers of slices per experiment are equal to 4, 6, 6, 7, and 8 for −400, −200, −100, +100, and +200 μA of DCS, respectively. Error bars correspond to SE.

RESULTS

Dendritic orientation does not determine whether DCS is inhibitory or excitatory. We recorded fEPSPs from basal and apical dendrites of CA1 pyramidal neurons by stimulation of stratum oriens association fibers and Schaffer collaterals, respectively. Roughly, these neuronal structures are oriented in opposing directions relative to CA1 soma and also relative to the DC vector. With cathodal DCS (cathode proximal to CA1 and anode proximal to CA3/dentate gyrus), we found robust amplitude-dependent fEPSP inhibition in both apical and basal CA1 dendrites, and the inhibition was stronger at higher DC amplitudes (Figs. 2 and 3). However, the degree of inhibition was different, e.g., at 200 μA cathodal DC, basal fEPSPs were inhibited by 67 $\pm$ 12% and apical by 16 $\pm$ 6% (no. of experiments and *P* values are presented in the legends of Figs. 1–7 as appropriate). Notably, the suppressive effect of 5 min of DCS was reversible, even when 400 μA cathodal DCS completely blocked basal dendrite fEPSPs (Fig. 2, *E* and *F*).

In contrast to the cathodal condition, 100 μA anodal DCS facilitated fEPSPs in both apical and basal dendrites. In apical dendrites, 100 μA anodal DCS significantly facilitated the fEPSPs by 9 $\pm$ 2% ($n = 5$, $P < 0.05$; Fig. 3*D*). The effect on basal dendrite fEPSPs was in the same direction, although not statistically different from the baseline. However, on average, 200 μA anodal DCS reduced apical fEPSPs by 9 $\pm$ 2% (Fig. 3*D*). Four hundred-microampere anodal DCS reliably produced epileptiform discharges in the slice, consistent with published reports of spontaneous neuronal activation by anodal DC and were therefore omitted from analysis (Chan et al. 1988).

PPF of the fEPSP supports a presynaptic DCS mechanism. Having found polarity-dependent modulation of the fEPSP by DCS, we next sought to identify whether this can be attributed to a presynaptic or postsynaptic process. With the DC field oriented along the CA1 apical dendrite axis and with stimulation of the Schafer collaterals, DCS (from -200 to $+200$ μA) has opposite effects on fEPSP slope and PPF of the fEPSPs (Fig. 4). The best linear fit of the PPF data (Fig. 4*C*) shows that, when DCS suppresses the first of the paired fEPSPs by 10%, the PPF ratio increases by 2.6 $\pm$ 0.03% ($P < 0.001$), and, when DCS increases fEPSPs by 10%, the PPF ratio decreases by 2.6 $\pm$ 0.03% ($P < 0.001$). In accordance with common interpretations of PPF changes, these data imply that presynaptic vesicular glutamate release may be modulated by DCS (Lange-Asschenfeldt et al. 2007; Martire et al. 2011; Schulz et al. 1994).

Axonal orientation determines whether DCS is inhibitory or excitatory. To more explicitly test the contribution of the presynaptic component and axonal orientation relative to the DC field vector, fEPSPs were evoked in CA1 and CA3 apical dendrites by stimulation of Schaffer collaterals or mossy fibers, respectively. These conditions approximate AP propagation in opposite directions relative to each other, and parallel or antiparallel to the DC vector (Fig. 5).

When the DC vector was in approximately the same direction as the AP propagation vector in Schaffer collaterals (Fig. 5*A*), but opposite to the AP vector in the mossy fibers (Fig. 5*B*), DCS significantly inhibited the CA1 fEPSPs but not the CA3 fEPSPs (Fig. 5*C*). However, when the direction of the DC vector was approximately antiparallel to the AP vector in the

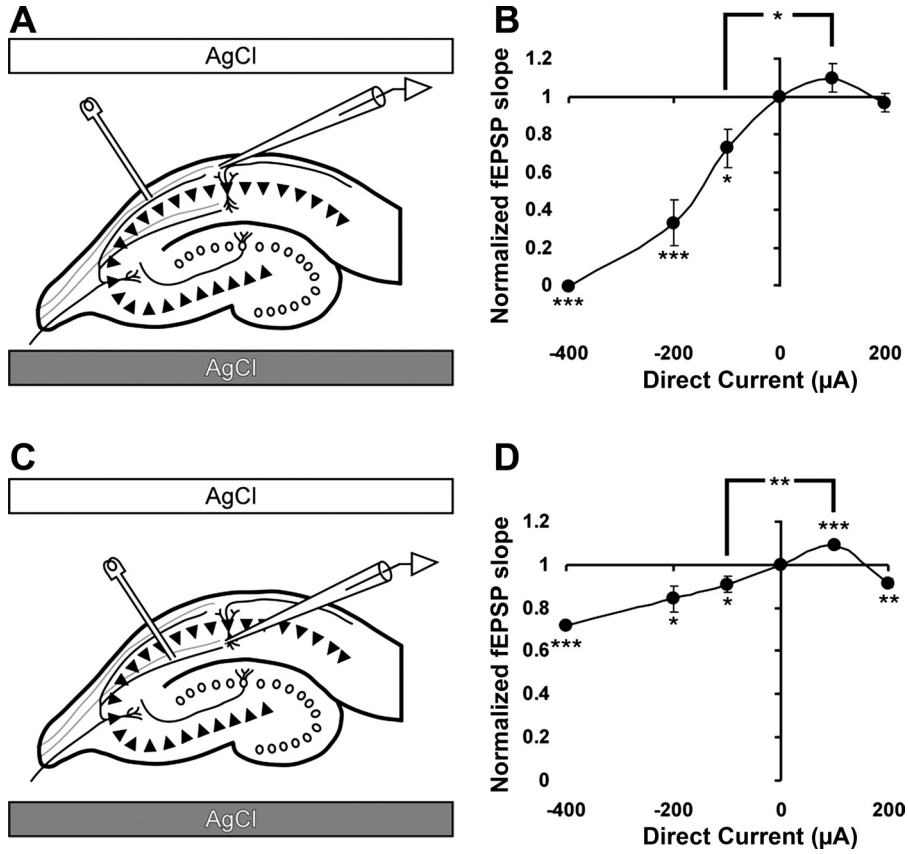

Fig. 3. DCS has similar effects on evoked fEPSPs in both basal and apical dendrites of CA1 neurons. *A* and *C*: positions of the DCS electrodes. Stimulating platinum-iridium (Pt-Ir) electrode is positioned at association fibers in stratum oriens in *A* and at Schaffer collaterals in *C*. The recording glass electrodes are positioned at basal or apical CA1 dendrites, respectively. *B*: the cumulative data based on the results shown in Fig. 2 reveal significant inhibition of fEPSPs in basal CA1 dendrites in all studied amplitudes of cathodal DCS. Values of fEPSP slope are 0, 33 $\pm$ 12, 75 $\pm$ 10, 110 $\pm$ 8, and 97 $\pm$ 5% for DCS of -400, -200, -100, $+100$, and $+200$ μA DCS, respectively. One-way ANOVA demonstrate significant dependence of average fEPSP slope on the DCS condition $F(4,26) = 25.6$; $P = 0.0001$. *D*: cathodal DCS also inhibits fEPSPs at apical dendrites of CA1 neurons. However, anodal DCS facilitates apical fEPSPs at 100 μA, but further increase in anodal DCS leads to inhibition of the fEPSPs. Values of fEPSP slope are 72 $\pm$ 1, 84 $\pm$ 6, 91 $\pm$ 4, 109 $\pm$ 2, and 91 $\pm$ 2% for DCS of -400, -200, -100, $+100$, and $+200$ μA, respectively. One-way ANOVA demonstrate significant dependence of average fEPSP slope on the DCS condition $F(4,22) = 7.77$; $P = 0.0005$. Numbers of slices are 3, 5, 10, 5, and 4 for -400, -200, -100, $+100$, and $+200$ μA of DCS, respectively. $^*P < 0.05$, $^{**}P < 0.01$, and $^{***}P < 0.001$.

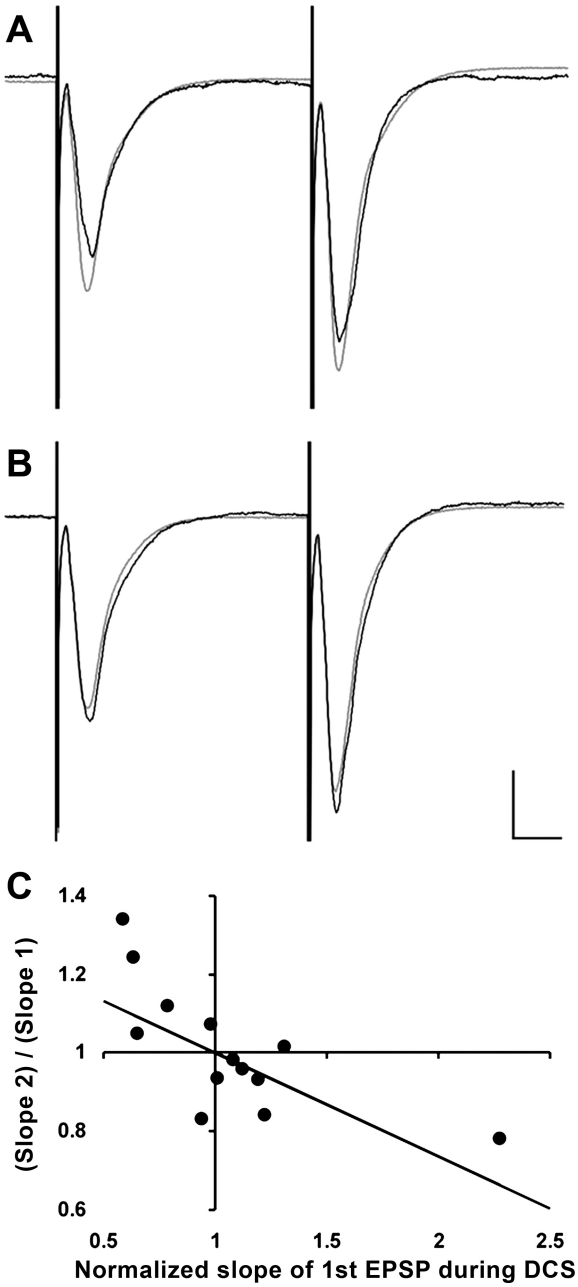

Fig. 4. DCS has opposite effects on fEPSP facilitation and paired-pulse facilitation (PPF) in CA1 apical synapses in electrodes' configuration shown in Fig. 3*C*. *A*: typically, cathodal DCS inhibits first fEPSP and increases the PPF ratio. *B*: anodal DCS facilitates first fEPSP but reduces the PPF ratio. In both cases, fEPSPs are in gray color before DCS and in black during DCS. fEPSPs after DCS were similar to those before DCS, as shown in Fig. 2, and they were omitted for clarity. The scaling bars are 500 μV and 10 ms, respectively. *C*: scatter plot and the best fit of the relationship between the changes in normalized PPF ratios and in changes in normalized fEPSPs caused by -200, -100, $+100$, or $+200$ μA DCS. PPF ratios during DCS were normalized to PPF ratios before DCS. In the absence of DCS, both normalized PPF ratios and normalized fEPSPs were equal to 1. Linear fit of the relationship in 8 hippocampal slices reveals significant negative correlation with a slope of -0.26 ± 0.03 ($P < 0.001$), which is in agreement with a presynaptic effect of DCS.

Schaffer collaterals, but approximately parallel to the mossy fiber AP vector, the DCS resulted in significant inhibition of CA3 fEPSPs but no CA1 fEPSP inhibition (Fig. 5*C*). Thus whether DCS is excitatory or facilitatory appears to depend on orientation of the DC vector relative to the efferent AP propagation vector and implies that the overall DCS effect on regional excitability is dependent on axonal orientation in the DC field rather than on dendritic orientation.

DCS modulates propagation of axonal excitation. To confirm DCS dependence on axonal orientation and therefore to also confirm a presynaptic DCS mechanism of action, we measured DCS effects on amplitude and delay time of CA1 population spikes generated by antidromic CA1 efferent axon stimulation (Fig. 6). When the DC vector was approximately perpendicular to the axonal vector, both negative and positive 200-μA DC polarities significantly decreased the amplitude by 16 ± 6 and 19 ± 4%, respectively ($P < 0.05$, Fig. 6). In this configuration, greater population spike inhibition corresponded to greater population spike delay, and the DCS effect was nearly symmetrical for both directions of the DC field vector (Fig. 6).

When CA1 axonal orientation was either parallel or antiparallel to the DC field, the effects of axonal orientation were, as with the fEPSP, polarity-dependent. A significant reduction in the population spike amplitude was recorded only when the AP propagation vector was oriented toward the cathode in a 100 ($P < 0.05$)-, 200 ($P < 0.01$)-, and 400 ($P < 0.01$)-μA DC field (Fig. 7). Notably, whereas, 100 μA DC parallel to the AP significantly inhibited both fEPSPs and population spikes, antiparallel 100-μA DC slightly facilitated or had no effect on either parameter (see Figs. 5*A*, filled circles in 5*C*, 7*A*, and 7*D*). Thus, depending on the relative efferent AP propagation vector, DCS similarly modulates both the fEPSPs and the antidromically excited population spikes, lending further support to an axonal contribution to the overall DCS effect on regional excitability.

DISCUSSION

We demonstrate for the first time that axonal orientation relative to the electric field vector determines whether DCS facilitates or suppresses regional neuronal excitability. Our findings complement previously described DCS-mediated neuronal cell body polarization (Bikson et al. 2004) and support the concept that neuromodulation in a homogenous electric field during tDCS in vivo is not uniform for all neurons in the stimulated brain volume.

One robust example of the DCS effect governed by axonal orientation to the DCS neuromodulatory effect is seen in the comparison of fEPSPs recorded in CA3 and CA1 after stimulation of the mossy fibers or the Schaffer collaterals, respectively. With stimulation of these two axonal pathways oriented approximately in opposite directions, application of a constant DCS polarity results in diametrically opposite effects on the postsynaptic response. The fEPSP is maximally suppressed when the AP travels toward the cathode and is either facilitated or remains unchanged when the excitatory signal propagates toward the anode (Fig. 5).

Although the fEPSP is a postsynaptic dendritic signal, paired-pulse stimulation data suggested a presynaptic component contributing to the DCS effect. Specifically, when cathodal DCS suppresses fEPSPs, it also increases the PPF ratio, a finding that is consistent with a presynaptic DCS mechanism of action. Thus, the PPF results imply that cathodal DCS reduces probability of glutamate release from presynaptic terminals,

and low anodal DCS has the opposite effect (Lange-Asschenfeldt et al. 2007; Martire et al. 2011; Schulz et al. 1994).

Because PPF data suggesting a presynaptic contribution to the DCS effect raise the possibility that DCS may affect axonal transmission, we investigated the axonal contribution to the DCS effect by antidromic stimulation of outgoing CA1 axons. With this setup, the resultant CA1 population spike amplitude is independent of synaptic transmission and therefore is a good indicator of the immediate effects of DCS on axonal excitation. Here, we find also a selective depression of the population spike when the excitatory signal is propagated toward the cathode and slight population spike facilitation when the signal is propagated toward the anode at 100 μA DCS. Notably, the antidromic axon stimulation data also show a predictable reduction in the population spike when the 200-μA DC and AP vectors are antiparallel to each other, which is consistent with an "anodal block" of axonal transmission due to significant hyperpolarization of cellular membrane closer to the anode (Rijkhoff et al. 1994; Vuckovic et al. 2005). The combined data in a two-dimensional summary diagram (Fig. 8) show the nonsymmetrical effect of DC that is either parallel or antiparallel to the AP vector, and symmetrical effects when the DC vector is perpendicular to the AP vector. It should be noted that, when low-level DC is parallel to AP, it causes maximum inhibition of the population spike amplitude, but it does not delay its peak time, whereas all other orientations delay the population spike peak time (Figs. 8, 6*E*, and 7*E*).

The relatively small inhibitory effect at approximately perpendicular orientation of DC and AP vectors can be explained by the high likelihood that, along any axon, the orientation of these two vectors is not exactly perpendicular, since any axon is not exactly linear and the inherent subtle curvature that would expose it to both parallel and antiparallel DC vector components. Therefore, at some points along the axon, the scalar product of the AC and DC vectors would be positive (leading to inhibiting effects) and in other areas negative (leading to facilitating effects). However, the inhibiting effects in general are stronger than the facilitating effects (Fig. 8), and therefore the total effect of both inhibiting and facilitating effects in the perpendicular DC field is small inhibition.

It should be noted that applied voltage during DCS might vary over time due to conductance changes at the ACSF-AgCl interface. In our experimental conditions, such voltage changes were not significant, and the voltage-current relationships remained linear at all studied DCS amplitude (Fig. 1). However, during DCS, the interface resistance might change, and we suggest that this should be taken into account, especially in prolonged protocols analogous to human tDCS.

In contrast to data demonstrating the critical contribution of axonal orientation, data obtained by recording fEPSP modulation in the apical and basal CA1 dendrite suggest that dendritic orientation in a DC field does not determine whether the DCS effect is excitatory or inhibitory, but in our experimental setup dendritic orientation does contribute to the magnitude of the DCS effect, particularly to the extent of fEPSP suppression by cathodal DCS (Figs. 2 and 3). The mechanism underlying the

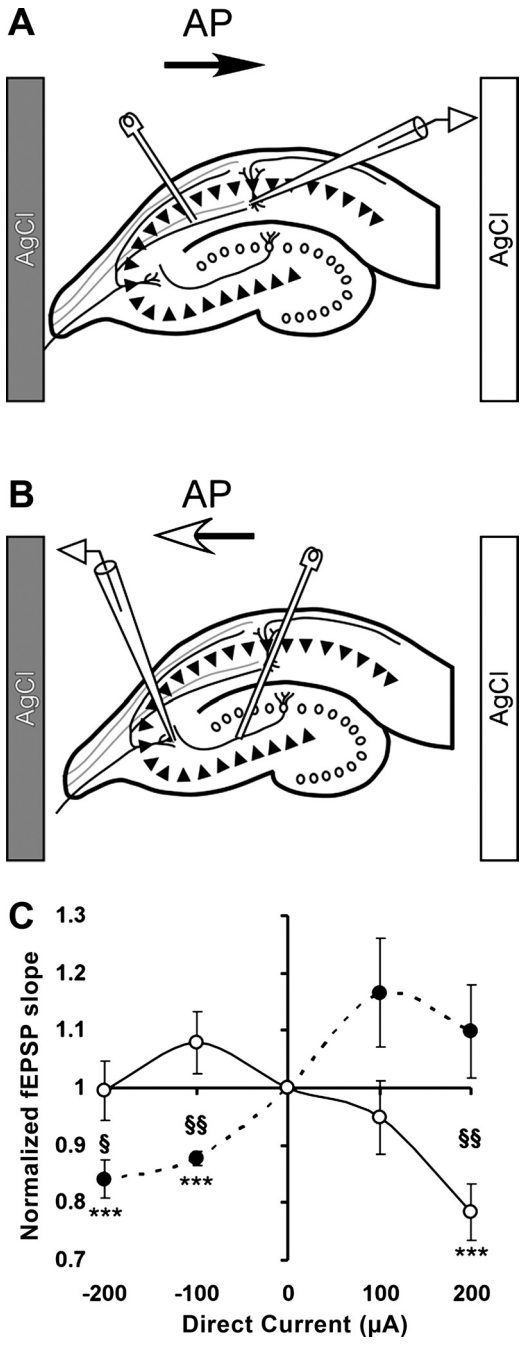

Fig. 5. DCS effect on fEPSPs in apical CA1 and CA3 dendrites depends on the direction of efferent action potential (AP) propagation vector. *A* and *B*: positions of the DCS electrodes and approximate directions of the vectors of AP in Schaffer collaterals (black head arrow) and in mossy fibers (white head arrow). Stimulating Pt-Ir electrode is positioned at Schaffer collaterals in *A* and at mossy fibers in *B*. The recording glass electrodes are positioned at apical CA1 and apical CA3 dendrites. Numbers of slices for CA1 fEPSPs (in *configuration A*) are 6, 6, 5, and 6 for -200, -100, $+100$, and $+200$ μA of DCS, respectively. Numbers of slices for CA3 fEPSPs (in *configuration B*) are 7, 6, 7, and 7 for -200, -100, $+100$, and $+200$ μA of DCS, respectively. *C*: effect of DCS on fEPSPs at apical dendrite CA1 neurons (filled circles) is opposite to the effect on fEPSPs at apical dendrite CA3 neurons (open circles). Values of fEPSP slope for CA1 region are 84 $\pm$ 3, 88 $\pm$ 1, 117 $\pm$ 9, and 110 $\pm$ 8% for DCS of -200, -100, $+100$, and $+200$ μA, respectively. One-way ANOVA confirms significant fEPSP dependence on the DCS condition $F(3,19) = 6.78$; $P < 0.003$. Values of fEPSP slope for CA3 region are 78 $\pm$ 5, 95 $\pm$ 6, 108 $\pm$ 5, and 99 $\pm$ 5% for DCS of -200, -100, $+100$, and $+200$ μA, respectively. As above, one-way ANOVA demonstrates significant contribution of the DCS condition to the fEPSP slope, $F(3,20) = 7.09$; $P = 0.002$. ***$P < 0.001$, difference from baseline. §$P < 0.05$ and §§$P < 0.01$, difference between CA1 and CA3 responses to DCS.

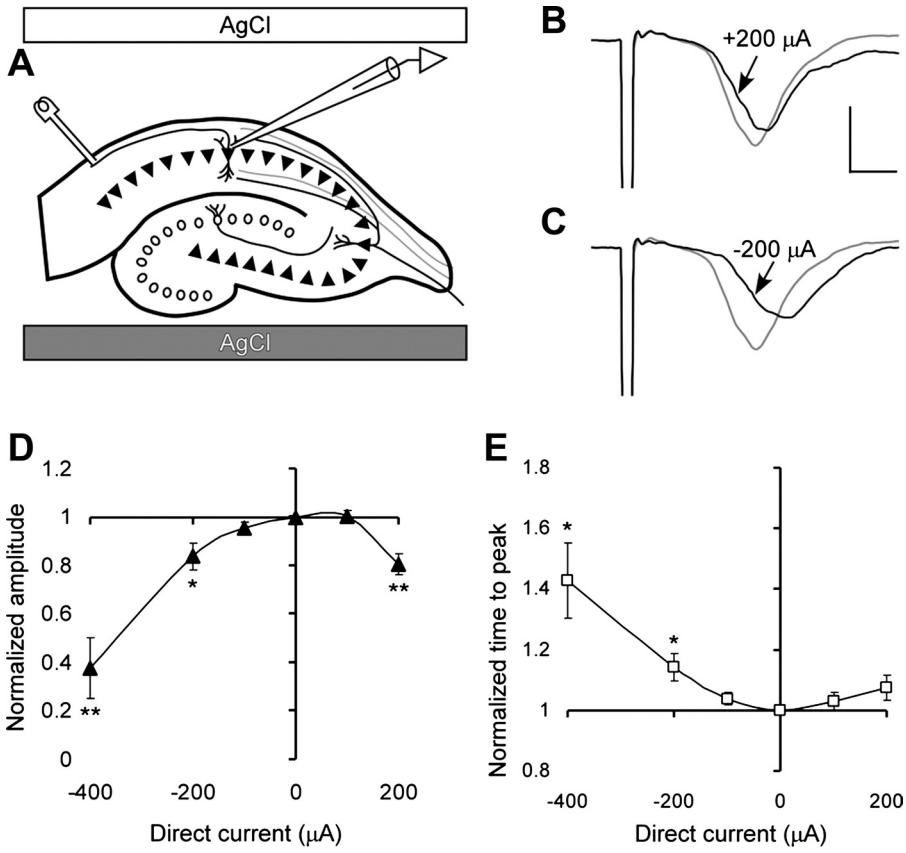

Fig. 6. Effect of DCS on population spikes in CA1 neurons stimulated antidromically when DCS current is approximately orthogonal to AP propagation. *A*: positions of DCS electrodes; Pt-Ir stimulating electrode is touching alveus, and tip of the glass recording electrode is in the CA1 layer. *B* and *C*: representative CA1 population spikes before (gray line) and during (black line) 200 μA of anodal and cathodal DCS, respectively. The scaling bars represent 1 mV and 1 ms, respectively. *D*: effect of DCS on normalized amplitude of the population spikes. Values of the spike amplitude are 38 $\pm$ 12, 84 $\pm$ 6, 95 $\pm$ 2, 100 $\pm$ 2, and 81 $\pm$ 4% for DCS of -400, -200, -100, $+100$, and $+200$ μA, respectively. One-way ANOVA demonstrate significant dependence spike amplitude on the DCS condition, $F(4,27) = 14.6$ and for $P < 0.0001$. Numbers of the slices per condition are 6, 7, 6, 7, and 6, respectively. *E*: effect of DCS on normalized time interval between the stimulus and the population spike. $^*P < 0.05$ and $^{**}P < 0.01$.

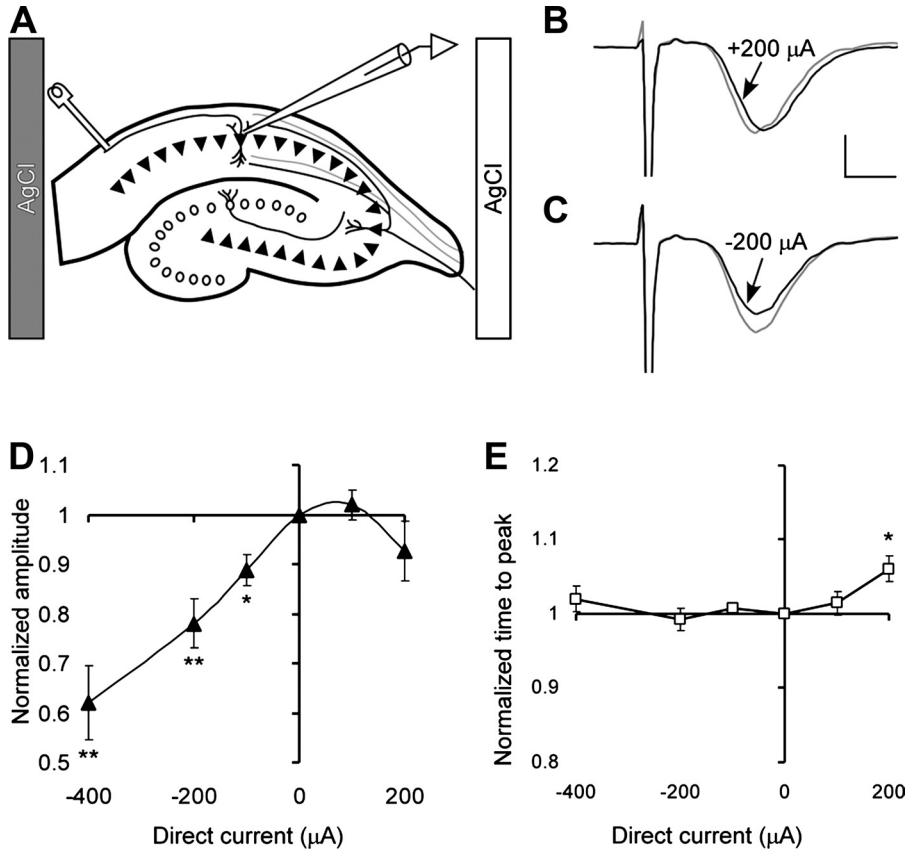

Fig. 7. Effect of DCS on population spikes in CA1 neurons stimulated antidromically when DCS current is approximately parallel or antiparallel to AP propagation. *A*: positions of the electrodes. *B* and *C*: representative CA1 population spikes before (gray line) and during (black line) 200 μA of anodal and cathodal DCS, respectively. The scaling bars represent 1 mV and 1 ms, respectively. *D*: effect of DCS on normalized amplitude of the population spikes. Values of the spike amplitude are 62 $\pm$ 7, 78 $\pm$ 5, 89 $\pm$ 3, 102 $\pm$ 3, and 93 $\pm$ 6% for DCS of -400, -200, -100, $+100$, and $+200$ μA, respectively. One-way ANOVA demonstrate significant dependence spike amplitude on the DCS condition, $F(4,23) = 8.8$; $P = 0.0002$. Numbers of the slices per condition are 6, 6, 5, 6, and 5, respectively. *E*: effect of DCS on normalized time interval between the stimulus and the population spike. $^*P < 0.05$ and $^{**}P < 0.01$.

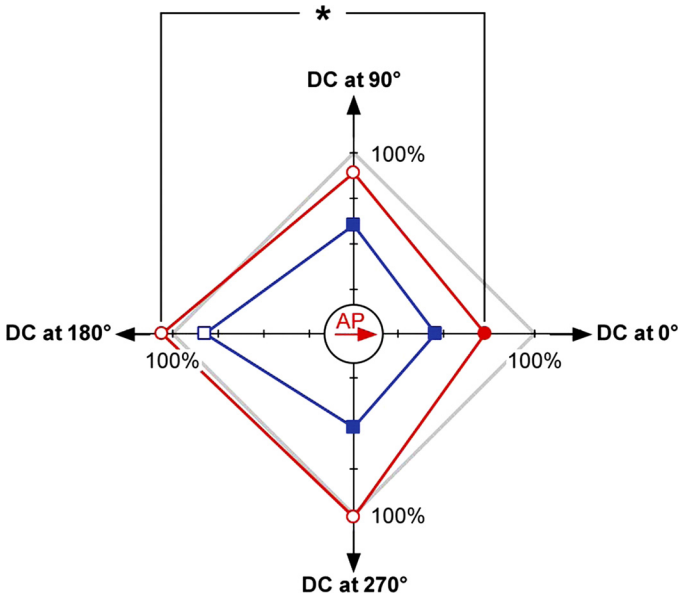

Fig. 8. Effect of DCS on CA1 population spike evoked by antidromic stimulation of CA1 neurons depends on the relative orientation of the DC current vector and the vector of the (AP) propagation. The diagram shows amplitudes of normalized amplitudes from Figs. 6*D* and 7*D* before DCS in gray (100%) and during 100- and 200-μA DCS as red circles and blue squares, respectively. The direction of the AP vector is shown as the red arrow in the origin (corresponding to 60%), and the directions of the DC current correspond to the back arrows at the ends of the axes (with ticks spaced at 10%). Filled circles and squares correspond to statistically significant effects on the amplitude. Open symbols correspond to nonsignificant variations. *$P < 0.05$ between the effects of 100-μA DC parallel and antiparallel to the AP propagation vector. Note that DCS always inhibits fEPSP when the vector projection of the AP propagation in the direction of the DC current is positive.

greater basal dendrite fEPSP suppression is not evident from our data. Plausibly, the grater magnitude may be due to deformation of the slice resulting from gravitational forces and redistribution of DC inside the slice, analogous to DC redistribution suggested by human tDCS models (Faria et al. 2009; Miranda et al. 2009). Alternatively, this discrepancy may be due to intrinsic physiological differences between the apical and basal CA1 synapses. These possibilities will ultimately have to be explicitly tested in follow-up studies, beyond the scope of this report.

Last, we address the biphasic effect of anodal stimulation in our setup. Specifically, we find a predictable pattern of mild excitatory signal facilitation by low (100 μA) anodal DCS but then mild suppression or return to neutral by 200 μA anodal DCS (e.g., Fig. 3*D*). One plausible explanation is the previously mentioned anodal block phenomenon. Another possibility is that the higher-amplitude anodal stimulation provokes spontaneous neuronal activity, perhaps even epileptiform activity, which may suppress the fEPSP around the time of seizure or other paroxysmal depolarization (Buckmaster and Wong 2002; Queiroz et al. 2009). Yet another intriguing explanation is that the reversal of DCS-mediated facilitation by increased DCS electrical current mimics the biphasic modulation of the motor-evoked potential by extending the time of anodal tDCS that was recently described in human trials (Monte-Silva et al. 2011). Given that the human phenomenon appears dependent on voltage-gated calcium channel activation, we hypothesize that high-current anodal DCS may result in an accumulation of intracellular calcium followed by perhaps prolonged opening of calcium-regulated potassium channels, as has been proposed for prolonged anodal tDCS in humans. In experiments beyond the scope of this study, we hope to address the mechanism of this phenomenon by further in vitro investigations and detailed pharmacology.

In conclusion, as tDCS gains acceptance in the clinical arena, we hope that our in vitro data will help in development of future tDCS applications as well as tDCS device design. Our finding of a strong contribution of axonal orientation to regional excitation or inhibition should enable hypothesis testing in vivo in both healthy subjects and in patients with abnormal cortical anatomy that has been disrupted by either a congenital or an acquired process. In such clinical instances, perhaps tDCS electrode positioning can be guided by tractography or related neuroimaging techniques that define axonal orientation in vivo. We conclude that further in vitro DCS studies are warranted and may contribute both to our knowledge of basic tDCS mechanisms and to improvement of day-to-day tDCS use.

GRANTS

This work was supported by the Children's Hospital Boston Translational Research Program (A. Rotenberg), National Institutes of Health (NIH) Grant K08 NS-055895 (A. Rotenberg), Department of Defense Medical Research and Development Program Basic Research Award PT090716 (A. Rotenberg and A. Y. Kabakov), the Center for Integration of Medicine and Innovative Technology (A. Rotenberg and A. Pascual-Leone), the RJG Foundation (A. Pascual-Leone), and NIH Grants 5R01NS-031718–19 (F. E. Jensen) and 5DP-1OD003347-04 (F. E. Jensen).

DISCLOSURES

No conflicts of interest, financial or otherwise, are declared by the authors.

AUTHOR CONTRIBUTIONS

A.R. conceived the research; A.Y.K. and A.R. designed the experiments; P.A.M. and A.R. collected pilot data; F.E.J. provided material support; A.Y.K. designed and built electrophysiological setup, performed all presented experiments, and analyzed the data; A.Y.K., F.E.J., A.P.-L., and A.R. interpreted the results; A.Y.K. prepared the figures; A.Y.K. and A.R. drafted the manuscript; all authors edited and revised manuscript.

REFERENCES

Antal A, Kriener N, Lang N, Boros K, Paulus W. Cathodal transcranial direct current stimulation of the visual cortex in the prophylactic treatment of migraine. *Cephalalgia* 31: 820–828, 2011.

Bikson M, Inoue M, Akiyama H, Deans JK, Fox JE, Miyakawa H, Jefferys JG. Effects of uniform extracellular DC electric fields on excitability in rat hippocampal slices in vitro. *J Physiol* 557: 175–190, 2004.

Bindman LJ, Lippold OC, Redfearn JW. The action of brief polarizing currents on the cerebral cortex of the rat (1) during current flow and (2) in the production of long-lasting after-effects. *J Physiol* 172: 369–382, 1964.

Brunoni AR, Ferrucci R, Bortolomasi M, Vergari M, Tadini L, Boggio PS, Giacopuzzi M, Barbieri S, Priori A. Transcranial direct current stimulation (tDCS) in unipolar vs. bipolar depressive disorder. *Prog Neuropsychopharmacol Biol Psychiatry* 35: 96–101.

Buckmaster PS, Wong EH. Evoked responses of the dentate gyrus during seizures in developing gerbils with inherited epilepsy. *J Neurophysiol* 88: 783–793, 2002.

Cambiaghi M, Teneud L, Velikova S, Gonzalez-Rosa JJ, Cursi M, Comi G, Leocani L. Flash visual evoked potentials in mice can be modulated by transcranial direct current stimulation. *Neuroscience* 185: 161–165, 2011.

Chan CY, Hounsgaard J, Nicholson C. Effects of electric fields on transmembrane potential and excitability of turtle cerebellar Purkinje cells in vitro. *J Physiol* 402: 751–771, 1988.

Dell'osso B, Zanoni S, Ferrucci R, Vergari M, Castellano F, D'Urso N, Dobrea C, Benatti B, Arici C, Priori A, Altamura AC. Transcranial direct current stimulation for the outpatient treatment of poor-responder depressed patients. *Eur Psychiatry* In press.

Faria P, Leal A, Miranda PC. Comparing different electrode configurations using the 10–10 international system in tDCS: a finite element model analysis. *Conf Proc IEEE Eng Med Biol Soc* 2009: 1596–1599, 2009.

Fujiwara T, Tsuji T, Honaga K, Hase K, Ushiba J, Liu M. Transcranial direct current stimulation modulates the spinal plasticity induced with patterned electrical stimulation. *Clin Neurophysiol* 122: 1834–1837, 2011.

Jensen FE, Wang C, Stafstrom CE, Liu Z, Geary C, Stevens MC. Acute and chronic increases in excitability in rat hippocampal slices after perinatal hypoxia in vivo. *J Neurophysiol* 79: 73–81, 1998.

Kamida T, Kong S, Eshima N, Abe T, Fujiki M, Kobayashi H. Transcranial direct current stimulation decreases convulsions and spatial memory deficits following pilocarpine-induced status epilepticus in immature rats. *Behav Brain Res* 217: 99–103, 2011.

Lange-Asschenfeldt C, Schipke CG, Riepe MW. Multimodal gain control at the hippocampal Schaffer collateral-CA1 synapse. *Neurosci Lett* 416: 101–105, 2007.

Lefaucheur JP, Antal A, Ahdab R, Ciampi de Andrade D, Fregni F, Khedr EM, Nitsche M, Paulus W. The use of repetitive transcranial magnetic stimulation (rTMS) and transcranial direct current stimulation (tDCS) to relieve pain. *Brain Stimulation* 1: 337–344, 2008.

Martire A, Tebano MT, Chiodi V, Ferreira SG, Cunha RA, Kofalvi A, Popoli P. Pre-synaptic adenosine A2A receptors control cannabinoid CB1 receptor-mediated inhibition of striatal glutamatergic neurotransmission. *J Neurochem* 116: 273–280, 2011.

McFadden JL, Borckardt JJ, George MS, Beam W. Reducing procedural pain and discomfort associated with transcranial direct current stimulation. *Brain Stimulation* 4: 38–42, 2011.

Miranda PC, Faria P, Hallett M. What does the ratio of injected current to electrode area tell us about current density in the brain during tDCS? *Clin Neurophysiol* 120: 1183–1187, 2009.

Monte-Silva K, Hessenthaler S, Kuo MF, Liebetanz D, Paulus W, Nische M. Induction of l-LTP-like plasticity in the human motor cortex by repeated non-invasive brain stimulation. In: *14th European Congress on Clinical Neurophysiology and 4th International Conference on Transcranial Magnetic and Direct Current Stimulation*. Rome, 2011.

Nitsche MA, Boggio PS, Fregni F, Pascual-Leone A. Treatment of depression with transcranial direct current stimulation (tDCS): a review. *Exp Neurol* 219: 14–19, 2009.

Nitsche MA, Paulus W. Excitability changes induced in the human motor cortex by weak transcranial direct current stimulation. *J Physiol 527 Pt* 3: 633–639, 2000.

O'Connell N, Wand B, Marston L, Spencer S, Desouza L. Non-invasive brain stimulation techniques for chronic pain. A report of a Cochrane systematic review and meta-analysis. *Eur J Phys Rehab Med* 47: 309–326, 2011.

Purpura DP, McMurtry JG. Intracellular activities and evoked potential changes during polarization of motor cortex. *J Neurophysiology* 28: 166–185, 1965.

Queiroz CM, Gorter JA, Lopes da Silva FH, Wadman WJ. Dynamics of evoked local field potentials in the hippocampus of epileptic rats with spontaneous seizures. *J Neurophysiol* 101: 1588–1597, 2009.

Rijkhoff NJ, Holsheimer J, Koldewijn EL, Struijk JJ, van Kerrebroeck PE, Debruyne FM, Wijkstra H. Selective stimulation of sacral nerve roots for bladder control: a study by computer modeling. *IEEE Trans Biomed Eng* 41: 413–424, 1994.

Sanchez RM, Koh S, Rio C, Wang C, Lamperti ED, Sharma D, Corfas G, Jensen FE. Decreased glutamate receptor 2 expression and enhanced epileptogenesis in immature rat hippocampus after perinatal hypoxia-induced seizures. *J Neurosci* 21: 8154–8163, 2001.

Schulz PE, Cook EP, Johnston D. Changes in paired-pulse facilitation suggest presynaptic involvement in long-term potentiation. *J Neurosci* 14: 5325–5337, 1994.

Vuckovic A, Struijk JJ, Rijkhoff NJ. Influence of variable nerve fibre geometry on the excitation and blocking threshold. A simulation study. *Med Biol Eng Comput* 43: 365–374, 2005.

Zaghi S, Heine N, Fregni F. Brain stimulation for the treatment of pain: a review of costs, clinical effects, and mechanisms of treatment for three different central neuromodulatory approaches. *J Pain Management* 2: 339–352, 2009.